Stochastic and complex depinning dynamics of magnetic domain walls

Joel Briones, François Montaigne, Michel Hehn, Daniel Lacour, Jeffrey R Childress, Matthew J Carey

PHYSICAL REVIEW B **83**, 060401(R) (2011)

Stochastic and complex depinning dynamics of magnetic domain walls

Joel Briones, François Montaigne, Michel Hehn, and Daniel Lacour
Institut Jean Lamour, CNRS, Nancy-Université, BP 70239, F-54506 Vandoeuvre lès Nancy, France

Jeffrey R. Childress and Matthew J. Carey
Hitachi San Jose Research Center, 3403 Yerba Buena Road, San Jose, California 95135, USA
(Received 3 November 2010; revised manuscript received 16 December 2010; published 10 February 2011)

We study the thermally induced depinning process of a single magnetic domain wall (DW) under applied field when the DW is trapped by a notch made in a nanowire shaped from a spin-valve multilayer with in-plane magnetization. In such devices depinning is typically a stochastic process and the depinning field distribution exhibits complex features. By analyzing simultaneously depinning field distributions and relaxation data, we observe two distinct sources of "complexity" in DW depinning processes: multiplicity in the DW structure and fundamental complexity in the depinning process.

DOI: 10.1103/PhysRevB.83.060401 PACS number(s): 75.78.Fg, 75.60.Ch, 75.70.Kw, 75.75.−c

Magnetic domain wall (DW) motion in magnetic nanowires is the focus of much research as it encompasses fundamental physical phenomena as well as the promise of novel magnetoelectronic applications. The motion of the DW can be initiated either by an external applied magnetic field or by a flow of current using spin-torque transfer. The position of the DW can be controlled by introducing pinning sites such as curved shapes, notches, protrusions, etc.[1–7] "Natural" defects in materials or structures are also a source of pinning and are of major importance in DW propagation,[8,9] and influence considerably the DW propagation and velocity. Understanding the phenomena of pinning and depinning of DW is therefore a key issue for both the study of DW motion as well as to optimize the design of DW-based devices.

It is recognized that the DW depinning process displays a stochastic behavior, highlighted by the observation of depinning field distributions (DFDs), finite depinning probability, or velocity distribution.[4,6,10–15] The observed depinning field distributions are often complex and contain several peaks. The stochastic behavior can be observed also in the time domain, at constant values of the external magnetic field and nanowire current. Relaxation measurements have characterized the distribution of DW depinning time in perpendicularly magnetized nanowires.[16] Telegraph noise owing to oscillations of a DW between two pinning sites have been reported also for perpendicular[17] and in-plane-magnetized pillars or nanowires.[18,19] These experiments reveal the exponential distribution of depinning times and are interpreted as resulting from thermal activation over a single energy barrier. Similarly to the well-known magnetization reversal of a single magnetic particle,[20] the characteristic activation time is described by an Arrhenius law, $\tau = \tau_0 \exp(\Delta E/k_B T)$. Here the energy barrier ΔE is a function of the applied magnetic field and of the current flowing through the DW. Such a model should result in a simple DFD with a single peak.[21] This is in contrast with a number of previously cited reports of complex DFDs.

The complex DFD behavior has been associated previously with the presence of different types of DWs injected into the nanowire,[7,15] which we will refer to as the "multiple injected DW" model. Within this model, several types of DW can be trapped in the notch, each one having its own dynamic [Fig. 1(b)] and contributing to the DFD. On the other hand, more complex relaxation dynamics in DW depinning have been observed by Attané *et al.*,[8] characterized by a depinning time distribution that is the sum of two exponentials with different characteristic times. The presence of these two times is interpreted using an "alternative paths" model schematized in Fig. 1(c). In this model, the depinning occurs either via a direct process (state 1 → state 3) or via an intermediate pinned state (state 2). The latter process is characterized by two successive transitions: 1 → 2 then 2 → 3. Each of these transitions is associated with a characteristic time: τ_{13}, τ_{12}, and τ_{23}. Such a process can in principle result in a complex (double-peak) distribution of depinning fields, although this has yet to be demonstrated experimentally. In this Rapid Communication we will show that a simultaneous analysis of both the relaxation dynamics *and* the DFD is necessary to provide a coherent analysis of complex depinning processes, and we will distinguish between the multiple injected DW and alternative paths models.

Samples studied in this Rapid Communication are identical to those analyzed in Ref. 13. The spin valve was grown by magnetron sputtering on a glass substrate with a structure (in nanometers) Ta(3)/Cu(2)/IrMn(6)/$Co_{65}Fe_{35}$(2.5)/Cu(3)/$Co_{65}Fe_{35}$(4)/$Ni_{86}Fe_{14}$(15)/Ru(6). The spin-valve film was patterned by electron-beam lithography and Ar-ion-beam etching in order to define a submicrometer wire 500 nm wide and 20 μm long, in which magnetic DWs can be created and manipulated. A large nucleation pad is present on one side of the wire and a sharp notch is positioned along the wire. Figure 1(a) shows a scanning electron microscopy picture of a completed device. Measurements of the overall giant magnetoresistance (GMR) in the nanowire (two-contact geometry) at room temperature allow the detection and precise positioning of the DW between the electrical contacts, and to study the depinning of the DW from the notch.

The DW nucleation occurs always in the nucleation pad, and for moderate values of the magnetic field H the notch acts as a pinning site and stops the DW propagation. A further increase in the field H is necessary to depin the DW. The stochastic behavior of the DW depinning from the notch has been

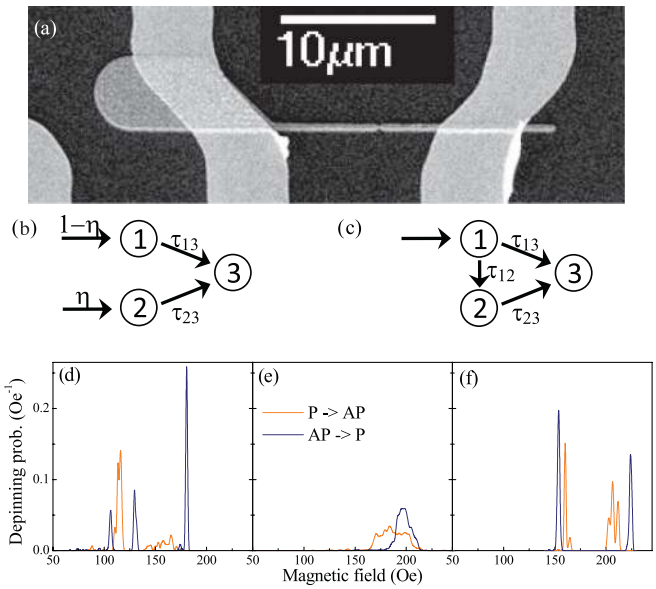

FIG. 1. (Color online) (a) Scanning electron microscopy view of the devices. (b) Scheme of the multiple injected DW model. (c) Scheme of the alternative paths model. (d)–(f) DFD of three different devices. Distributions are given for a parallel to antiparallel transition and vice versa.

studied by recording more than 1000 GMR loops. Histograms representing the DFD reveal complex features with multiple peaks of different shapes and widths. Furthermore, the DFD varies drastically from device to device, showing the extreme sensitivity to variations in devices (owing to subtle variations in device fabrication or in the local microstructure of the film). The analysis shows a systematic difference between propagation of head-to-head versus tail-to-tail DWs, owing to the stray magnetic field originating from the pinned magnetic layer of the spin valve.[13] Figures 1(d)–1(f) shows various examples of the resulting DFDs.

Here, DW depinning properties have been studied by measuring both DFD and relaxation data. In both experiments the DW is pinned in the notch by saturation of the magnetization, followed by the application of a reverse magnetic field. The pinning of the DW in the notch is verified by a nanowire resistance measurement, which quantifies the existence of opposite domains (representing the magnetization direction in the free layer of the spin valve) on each side of the notch. For depinning field measurements, the field is ramped at a rate of 2.5 Oe/s until the depinning is detected. For relaxation time measurement, the field is set to a fixed value and the depinning time is measured by monitoring the resistance every 100 ms. The cumulative depinning probability $P_3(t)$ (probability for the wall to be depinned at time t) is deduced from the depinning time distribution.

These two types of measurements are shown for a device (device A) in Figs. 2(a) and 2(b). The DFD is relatively simple, with two peaks [Fig. 2(a)]. Relaxation time measurements have been performed at fields close to the DFD peak values. At fields less than 200 Oe, the cumulative depinning probability varies exponentially with time and seems to saturate at a value of less than 1. On the other hand, at higher fields ($H > 200$ Oe), a high initial cumulative depinning probability is observed with a slow exponential saturation toward 1 as a function of time. In fact, the depinning probability can be expressed as a sum of two exponentials with very different time constants ($\tau_<$ and $\tau_>$). The proportion of each exponential is quantified by the proportion ratio r:

$$P_3(t) = 1 - (1-r)e^{-t\tau_<} - re^{-t\tau_>} (\text{with} \quad \tau_> \gg \tau_<). \tag{1}$$

Fitting of the relaxation data gives the evolution of r, $\tau_<$, and $\tau_>$ as a function of field. Remarkably, the proportion ratio r has a constant value (0.59). Both $\tau_<$ and $\tau_>$ have an exponential variation in the range of interest [Fig. 2(a)]. Such an evolution of the depinning probability can be explained by an alternative paths model, where the characteristic times of each transition can be deduced directly from experimental data:[8]

$$\begin{aligned} \frac{1}{\tau_{13}} &= \frac{1-r}{\tau_<} - \frac{1}{\tau_>} \approx \frac{1-r}{\tau_<}, \\ \frac{1}{\tau_{12}} &= \frac{1}{\tau_<} - \frac{1}{\tau_>} \approx \frac{1}{\tau_<}, \quad \text{and} \quad \tau_{23} = \tau_>. \end{aligned} \tag{2}$$

The DFD must be retrieved from the time evolution of the system given by

$$\frac{d\vec{P}(t)}{dt} = \begin{pmatrix} -\frac{1}{\tau_{12}} - \frac{1}{\tau_{13}} & 0 & 0 \\ \frac{1}{\tau_{12}} & -\frac{1}{\tau_{23}} & 0 \\ \frac{1}{\tau_{13}} & \frac{1}{\tau_{23}} & 0 \end{pmatrix} \vec{P}(t). \tag{3}$$

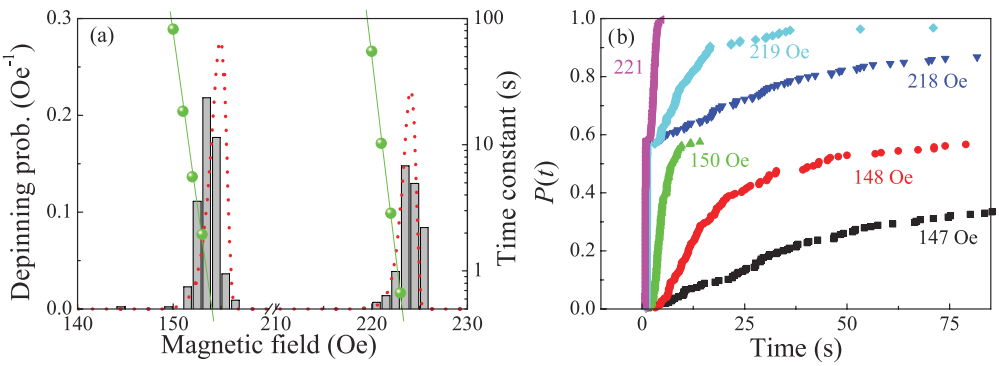

FIG. 2. (Color online) (a) DFD histogram for device A (column). Time constants deduced from (b) (dots). DFD deduced from the multiple injected DW model (dashed line). (b) Cumulated depinning probability for device A for different relaxation fields.

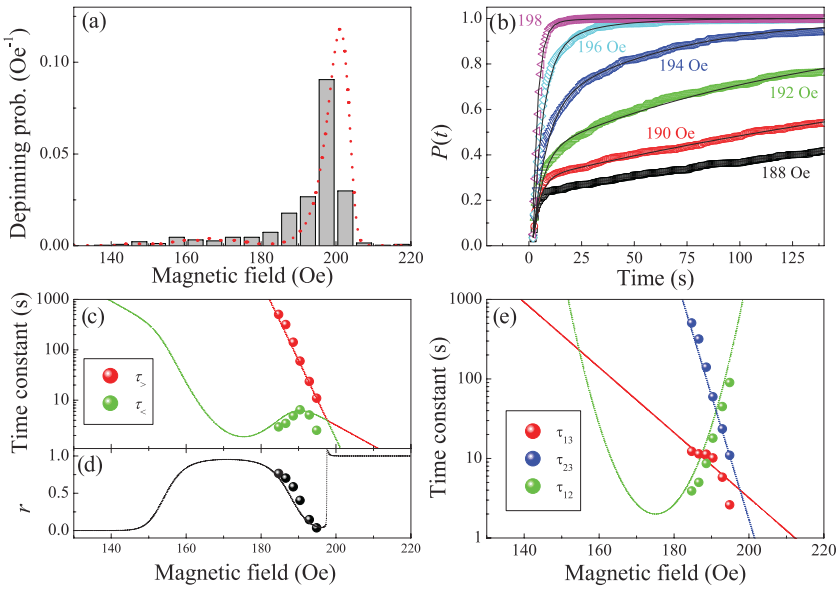

FIG. 3. (Color online) (a) DFD histogram for device B (column). DFD deduced from the alternative paths model (dashed line). (b) Cumulated depinning probability for device B for different relaxation fields. (c), (d) Parameters deduced from the fit to cumulated depinning probabilities (symbols). Para meters deduced from the alternative paths model (dashed line). (e) Parameters of the alternative paths model, deduced from relaxation data (symbols) and proposed modelization (dashed lines).

$\vec{P}(t)$ is a vector representing the probability for the system to be in each state (1,2,3). The initial condition is a DW in configuration 1: $\vec{P}(0) = (1,0,0)$.

Extrapolating the exponential field dependence of $\tau_<$ and $\tau_>$ and integrating the previous equation over a linear time variation of the magnetic field does not reproduce the observed DFD. On the contrary, the simulated distribution (not shown) exhibits mostly one peak. Indeed, in the whole field range it is found that $\tau_{12} < \tau_{13} \ll \tau_{23}$, so that the DW has a higher probability to switch to state 2 than to be depinned (state 3). The DFD contains only one peak associated with the $2 \rightarrow 3$ transition.

Rather than evoking the alternative paths model, the above behavior can be explained considering the multiple injected DW model [Fig. 1(b)]. Each type of DW has its own depinning dynamic, characterized by τ_{13} and τ_{23}. The proportion of each type of DW depends only on the injection process and is therefore field independent (it is quantified by $\eta = r$).

Figure 2(a) represents the DFD deduced from the integration of the following equation:

$$\frac{d\vec{P}(t)}{dt} = \begin{pmatrix} -\frac{1}{\tau_{13}} & 0 & 0 \\ 0 & -\frac{1}{\tau_{23}} & 0 \\ 0 & 0 & \frac{1}{\tau_{13}} + \frac{1}{\tau_{23}} \end{pmatrix} \vec{P}(t), \qquad (4)$$

with $\vec{P}(0) = (1-\eta,\eta,0)$.

The simulated DFD agrees well with the experimental data. The hypothesis of two different characteristic times associated with two different configurations of the pinned DW thus gives a coherent view of the depinning process.

Considering that the characteristic times are described by an Arrhenius law [$\tau = \tau_0 \exp(\Delta E/k_B T)$], the variation of the energy barrier is therefore linear. Such a variation can be interpreted as an effective Zeeman energy with $E(H) = E_0 - 2MVH$ (V being the effective volume of reversal). The slope of $\ln \tau(H)$ is thus $2MV/k_B T$. The two DWs have similar slopes, 1.24 and 1.45 Oe^{-1}, respectively, for τ_{13} and τ_{23} (these would result in an effective activation surface of $\sim$5 nm^2).

For device A, it has been shown that the set of experimental data can be interpreted by the presence of two different types of DW, together with thermally assisted depinning. Each type of DW has its own single energy barrier. Note that the occurrence of different injected magnetic configurations has been observed in other nominally identical devices.[22]

Let us consider now another device, device B, nominally identical to A. In that case the DFD is composed of only one peak with a broad shoulder extending to low depinning fields [Fig. 3(a)]. The cumulative distribution function of the depinning time [Fig. 3(b)] appears to be quite different from the one corresponding to device A [Fig. 2(b)]. Indeed, even if the cumulative distribution functions of the depinning time in Fig. 3(b) could be fitted also using two exponential decays $\tau_<$ and $\tau_>$, the proportion ratio r parameter in this case appears to be field dependent, as shown in Fig. 3(c). The two characteristic times can therefore not be attributed to the injection of two different DWs (which would imply a constant r value). Instead, the alternative paths model can in this case explain the observed depinning relaxation rate. Figure 3(e) shows the deduced τ_{12}, τ_{13}, and τ_{23}. The two characteristic times τ_{13} and τ_{23} corresponding to depinning of the DW from state 1 and state 2, respectively, logically decrease with the applied field. By contrast, τ_{12} *increases* with the applied field. A similar field dependence for τ_{12} has also been observed by Attané *et al.*[8] Such a result makes the model inconsistent with DFD. Indeed, a simple monotonous variation of τ_{12} at lower fields implies that the $1 \rightarrow 2$ transition is much more probable than the $1 \rightarrow 3$ transition. Starting at low fields, the system would thus switch from state 1 to state 2 and the depinning would occur only by the $2 \rightarrow 3$ transition. This would result in a *single peak* in the DFD, and is inconsistent with experimental data, which show a clear low-field shoulder in the depinning probability distribution [Fig. 3(a)]. To avoid such discrepancy, it is necessary to impose a nonmonotonous evolution of τ_{12} with the field. As an example, the model of characteristic times chosen in Fig. 3(e) (linear dependence on the field of

the barrier height for τ_{13} and τ_{23}, parabolic dependence for τ_{12}) gives a reasonable agreement with the experimental data. It reproduces qualitatively the DFD [dashed line in Fig. 3(a)] and the relaxation parameters deduced from the fit [dashed lines in Fig. 3(c)].

The effective Zeeman energy coefficients of the $1 \rightarrow 3$ and $2 \rightarrow 3$ transitions are, respectively, 0.11 and 0.42 Oe^{-1}, values somehow smaller than for device A. Furthermore, no simple physical mechanism explains the nonmonotonous variation of the barrier height for the transition $1 \rightarrow 2$. Nevertheless, possible explanations include resonant phenomena, fluctuations between state 1 and state 2, changes in the DW configuration with the applied field, or dynamical effects. It is also interesting to note that, despite the completely different nature of the DWs (planar versus perpendicular magnetization), Attané *et al*. have observed a similar variation of τ_{12}. These two separate observations might be the result of a universal, complex depinning mechanism.

In conclusion, we have described in this paper two examples of thermally activated complex mechanisms of DW depinning. In the first case, the complexity of the DFD arises from the presence of two different DW configurations at the notch. In the second case, a more complex scheme has to be invoked. Overall, a "two alternative paths" model can account reasonably for the whole data set, even though the exact mechanism behind the transition between the two paths remains unclear. This result highlights the fact that analyses of *both* the DFD *and* relaxation times are necessary to adequately describe thermally activated complex depinning processes. In particular, considering only relaxation time measurements might easily lead to misinterpretation.

The work presented in this article is partly supported by La Région Lorraine. J.B. acknowledges support from CONACYT. The authors acknowledge G. Lengaigne for technical assistance.

[1] T. Ono, H. Miyajima, K. Shigeto, and T. Shinjo, Appl. Phys. Lett. **72**, 1116 (1998).
[2] M. Kläui, C. A. F. Vaz, J. A. C. Bland, W. Wernsdorfer, G. Faini, and E. Cambril, Appl. Phys. Lett. **81**, 108 (2002).
[3] D. Petit, A.-V. Jausovec, D. Read, and R. P. Cowburn, J. Appl. Phys. **103**, 114307 (2008).
[4] M. Hayashi, L. Thomas, C. Rettner, R. Moriya, and S. S. P. Parkin, Appl. Phys. Lett. **92**, 162503 (2008).
[5] E. R. Lewis, D. Petit, L. Thevenard, A. V. Jausovec, L. O'Brien, D. E. Read, and R. P. Cowburn, Appl. Phys. Lett. **95**, 152505 (2009).
[6] M.-Y. Im, L. Bocklage, P. Fischer, and G. Meier, Phys. Rev. Lett. **102**, 147204 (2009).
[7] J. Akerman, M. Muñoz, M. Maicas, and J. L. Prieto, Phys. Rev. B **82**, 064426 (2010).
[8] J. P. Attané, D. Ravelosona, A. Marty, Y. Samson, and C. Chappert, Phys. Rev. Lett. **96**, 147204 (2006).
[9] V. Uhlíř, S. Pizzini, N. Rougemaille, J. Novotný, V. Cros, E. Jiménez, G. Faini, L. Heyne, F. Sirotti, C. Tieg, A. Bendounan, F. Maccherozzi, R. Belkhou, J. Grollier, A. Anane, and J. Vogel, Phys. Rev. B **81**, 224418 (2010).
[10] A. Himeno, T. Ono, S. Nasu, K. Shigeto, K. Mibu, and T. Shinjo, J. Appl. Phys. **93**, 8430 (2003).
[11] G. Meier, M. Bolte, R. Eiselt, B. Krüger, D.-H. Kim, and P. Fischer, Phys. Rev. Lett. **98**, 187202 (2007).
[12] P. Lendecke, R. Eiselt, G. Meier, and U. Merktet, J. Appl. Phys. **103**, 073909 (2008).
[13] J. Briones, F. Montaigne, D. Lacour, M. Hehn, M. J. Carey, and J. R. Childress, Appl. Phys. Lett. **92**, 032508 (2008).
[14] P. Möhrke, T. A. Moore, M. Kläui, J. Boneberg, D. Backes, S. Krzyk, L. J. Heyderman, P. Leiderer, and U. Rüdiger, J. Phys. D **41**, 164009 (2008).
[15] M. Hayashi, L. Thomas, C. Rettner, R. Moriya, X. Jiang, and S. S. P. Parkin, Phys. Rev. Lett. **97**, 207205 (2006).
[16] C. Burrowes, A. P. Mihai, D. Ravelosona, J.-V. Kim, C. Chappert, L. Vila, A. Marty, Y. Samson, F. Garcia-Sanchez, L. D. Buda-Prejbeanu, I. Tudosa, E. E. Fullerton, and J.-P. Attané, Nat. Phys. **6**, 17 (2010).
[17] J. Cucchiara, Y. Henry, D. Ravelosona, D. Lacour, E. E. Fullerton, J. A. Katine, and S. Mangin, Appl. Phys. Lett. **94**, 102503 (2009).
[18] S. Laribi, V. Cros, M. Muñoz, J. Grollier, A. Hamzić, C. Deranlot, A. Fert, E. Martínez, L. López-Díaz, L. Vila, G. Faini, S. Zoll, and R. Fournel, Appl. Phys. Lett. **90**, 232505 (2007).
[19] M. Eltschka, M. Wötzel, J. Rhensius, S. Krzyk, U. Nowak, M. Kläui, T. Kasama, R. E. Dunin-Borkowski, L. J. Heyderman, H. J. van Driel, and R. A. Duine, Phys. Rev. Lett. **105**, 056601 (2010).
[20] W. Wernsdorfer, E. B. Orozco, K. Hasselbach, A. Benoit, B. Barbara, N. Demoncy, A. Loiseau, H. Pascard, and D. Mailly, Phys. Rev. Lett. **78**, 1791 (1997).
[21] A. Garg, Phys. Rev. B **51**, 15592 (1995).
[22] F. Montaigne *et al.* (unpublished).